Journal of Sound and Vibration (1999) **228**(2), 397–420
Article No. jsvi.1999.2411, available online at http://www.idealibrary.com on IDEAL®

FINITE ELEMENT DYNAMIC MODEL UPDATING USING MODAL THERMOELASTIC FIELDS

L. HUMBERT, F. THOUVEREZ AND L. JEZEQUEL

Ecole Centrale de Lyon, Mechanical Engineering Department UMR 5513, 36 *avenue Guy de Collongue, Lyon* 69131, *France*

(*Received* 14 *December* 1998, *and in final form* 1 *June* 1999)

In this paper, the use of thermoelastic measurements to improve a finite element model is investigated. The originality of the procedure lies in the use of this stress sum field measurement and in the new solution method of the modelling error location stage. Measurement inaccuracies and expansion errors are taken into account through an inequality constraint. Finally, the correction stage is done owing to a variable metric Gauss–Newton method. This updating process has been applied to modal thermoelastic measurements carried out on a thin plate bending with different kinds of defects

1. INTRODUCTION

During the last 20 years, finite element model updating has focused much research, especially in the aeronautical and automotive industries. Many techniques have been proposed, but they were sometimes limited by the available experimental data. The development of high-performance acquisition systems, allowing an accurate and wide investigation of structure behaviour, revives the interest in this subject. In this paper, the thermoelastic measurement technique that provides the experimental dilatation field measurement for structures under harmonic loading [1, 2] will be considered. Despite its high sensitivity to local defects and its achievement of a stress field measurement, this technique is not yet widespread. This is mainly due to difficulties in the interpretation of such data.

Stress experimental values are rarely used for finite element model improvement, because of the difficulty to introduce stress data in standard updating schemes. Standard finite element models are built only with an approximation of the displacement field. The stresses are *a posteriori* computed by a derivation and a smoothing of the displacement field [3]. To bypass this difficulty, a mixed finite element approach, based on simultaneous approximation of displacement and stress fields [3, 4] has been chosen. This non-standard modelling allows easy handling of the thermoelastic measurement as well as all kinds of stress value in the iterative updating process.

Updating schemes can be classified into two categories [5]: direct correction methods and iterative correction methods. In the first one, models are only mass and stiffness matrices, which are adjusted in one step by a mathematical

0022-460X/99/470397 + 24 $30.00/0

approach [6, 7]. Models corrected in this manner have lost their physical meaning as well as their predictivity based on the updated frequency domain. In iterative methods, models are defined by a set of physical parameters on the finite element mesh. The updating is then achieved by an iterative two-step process, composed of an ill-modelled areas location and a correction of the corresponding parameters. These methods are heavier to implement, but preserve the physical meaning of the model. The most crucial step is the parameter choice which will determine the good or bad conditioning of the correction process. To help this choice some modelling error indicators have been developed, usually based on the equilibrium equation residual term [8] or the constitutive law error [9].

However, these procedures are quite sensitive to measurement errors or inaccuracies due to the usual resolution in a modal subspace [10]. A new approach to the error location problem is suggested in which these errors are managed by an inequality constraint on the measured data. The problem is solved by an interactive linearization of the distance between analytical and experimental data. In order to make the parameter selection easier, a correlation of the several modal error indicators is introduced. Finally, the correction stage is achieved owing to a variable metric Gauss–Newton method with a polynomial line search [11], applied to a cost function involving thermoelastic data and eigenfrequencies. Modal parameter sensitivities are computed by Fox's modal superposition method [12] adapted to the mixed finite element model.

The previously described approach has been applied to measurements carried out on thin plate bending with different kinds of defects. After a short description of the thermoelastic measurement, the error location results are discussed. The influence of the *a priori* error estimation is investigated, and the location of its range is reached. Lastly, the model is corrected towards mass parameters and boundary stiffnesses.

2. FINITE ELEMENT MODELLING

The mixed model used in this paper is built with a Hellinger–Reissner principle involving simultaneously the displacement and stress fields. It consists in finding the real fields (u_i, σ_{ij}) which make the following function steady:

$$\mathscr{F}_R(u_i, \sigma_{ij}) = \int_\Omega (-W_c(\sigma_{ij}) - f_i u_i + 1/2\sigma_{ij}(u_{i,j} + u_{j,i}) - 1/2\rho\omega^2 u_i^2)\,\mathrm{d}\Omega$$
$$- \int_{\Gamma_\sigma} t_i^0 u_i\,\mathrm{d}\Gamma_\sigma - \int_{\Gamma_u} \sigma_{ij} n_j (u_i - u_i^0)\,\mathrm{d}\Gamma_u. \tag{1}$$

This principle describes explicitly the equilibrium equation, the constitutive law and all the boundary conditions which can be restored by differentiating the above expression. It must be underlined that, in the standard displacement formulation, the only explicit relations are the equilibrium equation and the kinematic boundary conditions. All other mechanical relations are implicitly used but are not enforced by the variational principle and thus will not be represented by a finite element relation.

Once the structure has been discretized with finite elements, the mechanical fields are approximated on each element (e) owing to their values (degrees of freedom) at the nodes n by

$$u^{(e)}(x, y, z) = \sum_n N_{un}^{(e)}(x, y, z)\bar{u}_n^{(e)}, \qquad \sigma^{(e)}(x, y, z) = \sum_n N_{\sigma n}^{(e)}(x, y, z)\bar{\sigma}_n^{(e)}.$$

In these relationships, N_u, N_σ are appropriate shape functions and $\bar{u}$, $\bar{\sigma}$ the corresponding displacement and stress degrees of freedom vectors, that have to be determined. The substitution of approximated fields in the Hellinger–Reissner principle and its computation for each finite element provide a quadratic matrix function. Finally, the steady state conditions of this function versus displacement and stress degrees of freedom provide the following equations which respectively correspond to the equilibrium equation and the constitutive law:

$$\begin{pmatrix} -\omega^2\mathbb{M} & \mathbb{K}_1 \\ \mathbb{K}_1^t & \mathbb{K}_2 \end{pmatrix} \begin{pmatrix} \bar{\mathbf{u}} \\ \bar{\boldsymbol{\sigma}} \end{pmatrix} = \begin{pmatrix} \mathbf{F} \\ \mathbf{0} \end{pmatrix}. \tag{2}$$

All of the elementary matrices needed to build this system are given in Appendix A. This set of equations is rarely solved in this form, especially for the eigenvectors computation. The constitutive law can be used to express stresses in terms of displacements:

$$\bar{\sigma} = \mathbf{H}\mathbf{D}\bar{\mathbf{u}} = -\mathbb{K}_2^{-1}\mathbb{K}_1^t\bar{\mathbf{u}} \tag{3}$$

and then, after substituting relation (3) into relation (2), the standard eigenvalue equation is obtained:

$$(\mathbb{K} - \omega^2\mathbb{M})\bar{\mathbf{u}} = \mathbf{0} \quad \text{with } \mathbb{K} = -\mathbb{K}_1\mathbb{K}_2^{-1}\mathbb{K}_1^t. \tag{4}$$

These relationships only involve diagonal or very sparse matrices, which make the computation quite easy. Relation (4) allows one to compute eigenmodes (ω_k, ϕ_k) and by using equation (3) the corresponding stress vectors Σ_k.

3. THERMOELASTIC EFFECT

The so-called thermoelastic effect is the adiabatic temperature change due to the material dilatation. It was investigated by Lord Kelvin over a hundred years ago, but the infrared camera technology has allowed one to measure it for only 20 years. The thermoelasticity in comparison with the elasticity, requires an additional variable, the temperature, which introduces additional effects. Thermoelastic equations consist of the motion equation (5), whose expression is already unchanged, and the heat conduction equation (6):

$$\rho\frac{\partial^2 u_i}{\partial t^2} = \sigma_{ij,j} + f_i \tag{5}$$

$$\rho c_\varepsilon\frac{\partial\theta}{\partial t} = r + k\theta_{,ii} - 3K\alpha T\frac{\partial\varepsilon_{ii}}{\partial t} \tag{6}$$

with a linear elastic and isotropic constitutive law

$$\sigma_{ij} = \lambda \varepsilon_{kk} \delta_{ij} + 2\mu \varepsilon_{ij} - 3K\alpha\theta\delta_{ij}. \tag{7}$$

The r and $k\theta_{,ii}$ terms denote the external heat supply and the heat conductivity. They can be neglected by assuming that an elementary material particle has a quasi-adiabatic behaviour when frequency is beyond a few Hertz [2]. Furthermore, as one is dealing with small changes around ambient temperature, the temperature term in the constitutive law (7) can also be neglected. The heat equation may be simplified as follows:

$$\rho c_\varepsilon \frac{\partial \theta}{\partial t} = -3K\alpha T \frac{\partial \varepsilon_{ii}}{\partial t}. \tag{8}$$

The expression of the temperature change in terms of the sum of the principal stresses or the sum of the principal strains is given by

$$\Delta\theta = -\frac{3K\alpha T}{\rho c_\varepsilon} \Delta tr\, \varepsilon = -\frac{\alpha T}{\rho c_\sigma} \Delta tr\, \sigma. \tag{9}$$

This measurement has been investigated in detail in references [1, 2]. More details about the measurement system, discrimination capacity and accuracy will be given in the experimental part of this paper. Before being used in the updating process, this measure of a physical phenomenon must be transformed into finite element data.

The thermoelastic field $\Delta\theta$ is given on a rectangular grid of discrete measurement points p_i on the structure top surface (Figure 1). So, an efficient use of full-field experimental data requires a preliminary correlation between the tested structure and the modelled geometry. Once the measured field has been located on the mesh, the measurement can be projected on to the model. This is achieved by minimizing the distance between the experimental values and the corresponding finite element approximated field:

$$\min_{tr\,\sigma_m} \sum_{pi} \left\| -\frac{\rho c_\sigma}{\alpha T} \Delta\theta^{(pi)} - N_\sigma(x_{pi}, y_{pi}, z_{pi})\, t\bar{r}\, \sigma_m \right\| \tag{10}$$

or

$$\min_{tr\,\varepsilon_m} \sum_{pi} \left\| -\frac{\rho c_\varepsilon}{3K\alpha T} \Delta\theta^{(pi)} - N_\varepsilon(x_{pi}, y_{pi}, z_{pi})\, t\bar{r}\, \varepsilon_m \right\| \tag{11}$$

The mesh refinement must be suited to the measurement point density to obtain a well-conditioned problem. Now the finite element vectors $t\bar{r}\,\varepsilon_m$ or $t\bar{r}\,\sigma_m$ are considered as being the experimental data and can be handled with finite element governing equations. This projection smooths in part measurement inaccuracies.

4. MODELLING ERROR LOCATION

The measurement provides only limited experimental information, whereas the structure is modelled by a number of parameters (elementary mass and stiffness, geometry parameters, boundary stiffnesses, etc.). The parameter choice is a crucial

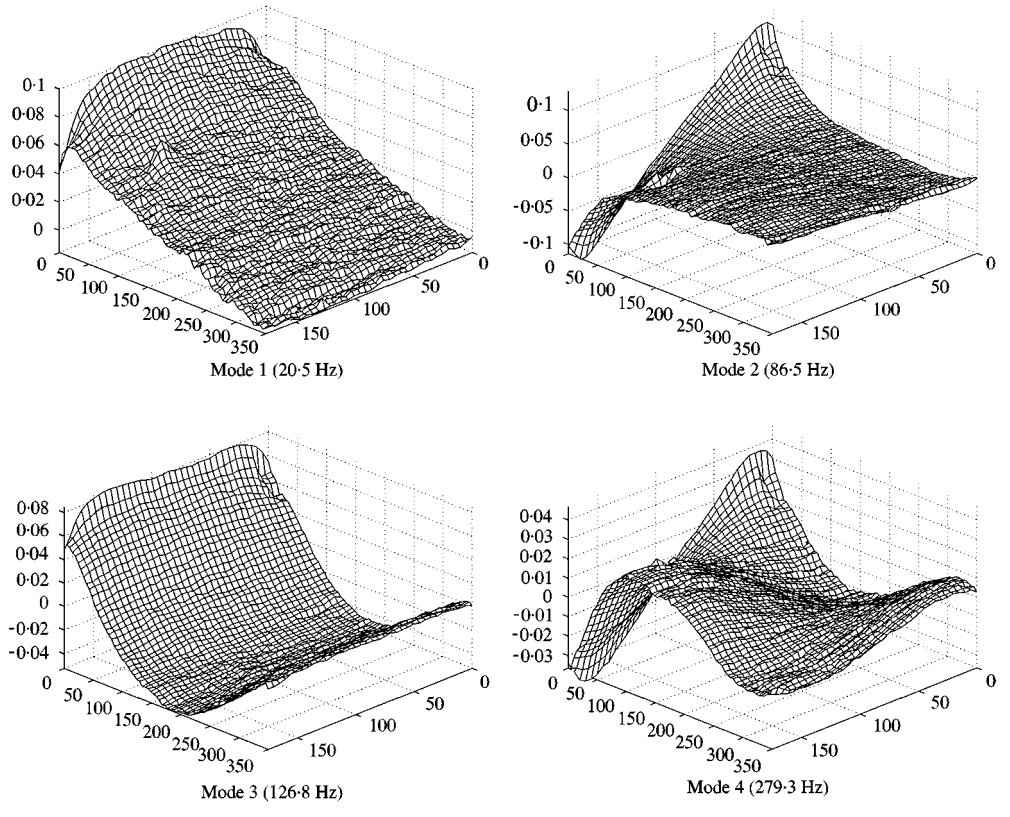

Figure 1. Thermoelastic measurement $\Delta\theta(K)$.

step which will determine the good or bad conditioning of the optimization problem. To help the user in this choice, some modelling error location techniques exist, often based on residual forces in the equilibrium equation or on the constitutive law error.

4.1. STANDARD ERROR LOCATION TECHNIQUES

The finite element model is characterized by the equilibrium relationship, the so-called eigenvalue equation:

$$(\mathbb{K} - \omega_k^2 \mathbb{M})\boldsymbol{\phi}_k = \mathbf{0}. \tag{12}$$

If the measurement provides the experimental circular eigenfrequency ω_{km} and the full deformation shape $\boldsymbol{\phi}_{km}$, one can substitute these values into the previous relationship:

$$(\mathbb{K} - \omega_{km}^2 \mathbb{M})\boldsymbol{\phi}_{km} = \mathbf{R}_k. \tag{13}$$

The equilibrium is not satisfied yet and a residual term $\mathbf{R}_k$ appears, representing the loading that has to be applied to the modelled structure to obtain the experimental

deformation shape. This vector can be straight linked to the mass and stiffness correction matrices by

$$\mathbf{R}_k = (-\Delta\mathbb{K} - \omega_{km}^2 \Delta\mathbb{M})\boldsymbol{\phi}_{km}. \tag{14}$$

Thus, this residual term may be used to locate the modelling inaccuracies. However, mode shapes are usually only measured at some discrete points and in particular directions of the experimental structure. Before the error location step, a reduction of the model for the measured degrees of freedom or an expansion of the experimental results for the whole model must be carried out [5]. Reduction techniques modify the model connectivity and lead to a propagation of the error in the whole matrices [8]. An expansion is, in the present case, far more suitable [5]. For a displacement u_m measured at some discrete points, the location problem is generally achieved by minimizing a cost function involving the residual forces and measured values:

$$\min_u \|(\mathbb{K} - \omega_m^2 \mathbb{M})\bar{\mathbf{u}}\|^2 + p|||\boldsymbol{\Pi}_m \bar{\mathbf{u}} - \bar{\mathbf{u}}_m|||^2. \tag{15}$$

Norms $\| \dots \|^2$ and $||| \dots |||^2$ usually have the physical meaning of the strain energy and so both terms have a similar weight. The weighting parameter p allows the measured data to be more or less enforced, depending on their reliability. The solution of this problem provides the expanded displacement vector $\bar{\mathbf{u}}$ and, by substituting it in the equilibrium equation (13), the residual vector for all degrees of freedom. Then an error indicator can be computed by estimating the residual forces for each finite element or substructure (e):

$$\eta_k^{(e)} = \|R_k\|_{(e)}^2 = R_k^{(e)t} U_k^{(e)} \quad \text{with } \mathbb{K}\mathbf{U}_k = \mathbf{R}_k. \tag{16}$$

This method is often considered to be very sensitive to measurement errors and conditioning problems [8].

Another widely used technique for detecting modelling inaccuracies is the constitutive law error method, developed by Ladeveze [9]. Its strong physical meaning gives it a good robustness to measurement error. The constitutive law error is defined as follows:

$$E^2(u, \sigma) = \int_\Omega \|\boldsymbol{\sigma} - \mathbf{HDu}\|^2 \, \mathrm{d}\Omega = \int_\Omega (\boldsymbol{\sigma} - \mathbf{HDu}) : \mathbf{Du} \, \mathrm{d}\Omega, \tag{17}$$

$$\mathbf{u} \in \mathscr{V}(\Omega) = \{\mathbf{u} \text{ regular}, \mathbf{u} = \mathbf{0} \text{ on } \Gamma_u\},$$

$$\boldsymbol{\sigma} \in \mathscr{S}(u, \Omega) = \{\boldsymbol{\sigma} = \mathbf{0} \text{ on } \Gamma_\sigma, \operatorname{div} \boldsymbol{\sigma} = \rho\ddot{u}\}.$$

This estimator provides the distance between the statistically admissible stress $\boldsymbol{\sigma}$ and the one computed with the constitutive law from the kinematical admissible displacement field $\mathbf{u}$. For the Hellinger–Reissner mixed model (3), its expression is given by

$$E^2(\bar{u}, \bar{\sigma}) = (\bar{\boldsymbol{\sigma}} + \mathbb{K}_2^{-1}\mathbb{K}_1^t \bar{\mathbf{u}})^t \mathbb{K}_1^t \bar{u} \tag{18}$$

with

$$\mathbb{K}_1\bar{\sigma} - \omega^2\mathbb{M}\bar{\mathbf{u}} = 0 \tag{19}$$

The statistical admissibility of the stress field introduces a relationship (19) between stress and displacement vectors: the equilibrium equation. Usually, a displacement field $\mathbf{v}$ is assigned to the stress field $\boldsymbol{\sigma}$ using the constitutive law.

$$\boldsymbol{\sigma} = \mathbf{HD}\mathbf{v} \Rightarrow \bar{\boldsymbol{\sigma}} = -\mathbb{K}_2^{-1}\mathbb{K}_1^{t}\bar{\mathbf{v}} \tag{20}$$

Thus, the expression of constitutive law error (18) becomes

$$E^2(\bar{u}, \bar{v}) = \|\bar{\mathbf{u}} - \bar{\mathbf{v}}\|^2 = (\bar{\mathbf{u}} - \bar{\mathbf{v}})^{t}\mathbb{K}(\bar{\mathbf{u}} - \bar{\mathbf{v}}) \tag{21}$$

As in the previous approach, the location problem can be expressed as a minimization problem involving the constitutive law error and the experimental data:

$$\min_{\bar{u}, \bar{v}} \|\bar{\mathbf{u}} - \bar{\mathbf{v}}\|^2 + p|||\boldsymbol{\Pi}_m\bar{\mathbf{u}} - \mathbf{u}_m|||^2$$

with

$$\mathbb{K}\bar{\mathbf{v}} - \omega_m^2\mathbb{M}\bar{\mathbf{u}} = \mathbf{0} \tag{22}$$

After the solution of this problem, the location is done using an element by element location of the constitutive law error:

$$\eta_k^{(e)} = \|\bar{\mathbf{u}} - \bar{\mathbf{v}}\|_{(e)}^2 = (\bar{\mathbf{u}}_k^{(e)} - \bar{\mathbf{v}}_k^{(e)})^{t}\mathbb{K}^{(e)}(\bar{\mathbf{u}}_k^{(e)} - \bar{\mathbf{v}}_k^{(e)}). \tag{23}$$

In the literature [8], both approaches are often contrasted, according to criteria such as robustness and accuracy. It can easily be demonstrated that if the norm $\|\ldots\|^2$ is built with the stiffness matrix, both problems are similar. For a given displacement vector $\bar{\mathbf{u}}$, the equilibrium equation residual vector and the constitutive law error are defined as follows:

$$\mathbf{R} = (\mathbb{K} - \omega_m^2\mathbb{M})\bar{\mathbf{u}},$$

$$E^2(\bar{\mathbf{u}}, \bar{\mathbf{v}}) = (\bar{\mathbf{u}} - \bar{\mathbf{v}})^{t}\mathbb{K}(\bar{\mathbf{u}} - \bar{\mathbf{v}}),$$

with

$$\mathbb{K}\bar{\mathbf{v}} = \omega_m^2\mathbb{M}\bar{\mathbf{u}}$$

from which one can deduce that the constitutive law error is equal to the energy of the residual forces:

$$\mathbf{R} = \mathbb{K}(\bar{\mathbf{u}} - \bar{\mathbf{v}}) \Rightarrow \mathbf{R}^{t}\mathbb{K}^{-1}\mathbf{R} = E^2(\bar{\mathbf{u}}, \bar{\mathbf{v}}). \tag{24}$$

4.2. ERROR LOCATION USING THERMOELASTIC DATA

For a standard finite element model dealing with stress values is tricky, because there exists no finite element relationship linking these data to the displacement

vector. But using the constitutive law operator built with a Hellinger–Reissner model (3), experimental stress values can be easily introduced into this location process. For thermoelastic measurement the constitutive law error problem can be expressed as follows:

$$\min_{\bar{u},\bar{v}} \|\bar{\mathbf{u}} - \bar{\mathbf{v}}\|^2 + p|||\mathbf{\Pi}_m Tr\,\mathbf{H}\mathbf{D}\bar{\mathbf{v}} - t\bar{r}\,\boldsymbol{\sigma}_m|||^2 \quad \text{with } \mathbb{K}\bar{\mathbf{v}} - \omega_m^2 \mathbb{M}\bar{\mathbf{u}} = \mathbf{0}. \tag{25}$$

Experimental data are as usual introduced by a weighting factor that allows them to be more or less applicable. The solution is directly determined by this parameter, which has no physical meaning and whose choice, according to the measurement reliability, is not straightforward. The most natural way to manage experimental data is to constrain them with the estimated measurement error ε_m. The location problem, then becomes, a minimization problem with an inequality constraint.

$$\min_{\bar{u},\bar{v}} (\bar{\mathbf{u}} - \bar{\mathbf{v}})^t \mathbf{K}(\bar{\mathbf{u}} - \bar{\mathbf{v}}) \quad \text{with } \mathbf{K}\bar{\mathbf{v}} - \omega_m^2 \mathbb{M}\bar{\mathbf{u}} = \mathbf{0}, \tag{26}$$

The norm here is a Euclidian one. Measurement inaccuracies mainly depend on the measurement technique and the care taken in measuring. They can reach 5–20%. For industrial models, the solution of problems (25) or (26) with respect to all degrees of freedom can sometimes be very cumbersome. So location problems are usually solved in the subspace of the q first analytical modes.

$$\bar{\mathbf{u}} = \mathbf{\Phi}\mathbf{a} = \sum_{i=1}^{q} \boldsymbol{\phi}_i \mathbf{a}_i, \qquad \bar{\mathbf{v}} = \mathbf{\Phi}\mathbf{b} = \sum_{i=1}^{q} \boldsymbol{\phi}_i \mathbf{b}_i, \tag{27}$$

$$\boldsymbol{\phi}_j^t \mathbf{K} \boldsymbol{\phi}_i = \delta_{ij}, \qquad \boldsymbol{\phi}_j^t \mathbf{M} \boldsymbol{\phi}_i = \frac{\delta_{ij}}{\omega_i^2}.$$

The unknown parameters are now the modal coefficients a_i and b_i. However, this resolution into a subspace is another important cause of error. Experimental results have shown (Table 1) that this error can reach 10% and must therefore be taken into account in the resolution process. The enforced error ε_m must be greater than the projection error; otherwise the problem has no solution. This error can be estimated by an evaluation of the distance between the experimental field and its least mean-square projection on the modal subspace:

$$\varepsilon_p = \frac{\|\mathbf{\Pi}_m \mathscr{T}\mathbf{a} - t\bar{r}\,\boldsymbol{\sigma}_m\|}{\|t\bar{r}\,\boldsymbol{\sigma}_m\|}, \tag{28}$$

TABLE 1

Modelling and projection errors

Mode		1	2	3	4
Modelling error	ε_0 (%)	18·2	35·2	15·2	30·3
Projection error	ε_p (%)	11·8	13·7	8·9	11·9

with

$$\mathbf{a} = (\mathscr{T}^{\mathrm{t}}\mathbf{\Pi}_m^{\mathrm{t}}\mathbf{\Pi}_m\mathscr{T})^{-1}(\mathbf{\Pi}_m\mathscr{T})^{\mathrm{t}}t\bar{r}\,\boldsymbol{\sigma}_m, \quad \mathscr{T} = Tr\mathbf{HD\Phi} = Tr\,\Sigma.$$

$\mathscr{T}$ denotes the stress sum matrix of the q first modes. By substituting equation (27) into equation (26) and using the orthogonal properties of the modes, the location problem can be expressed only in terms of coefficients a_i:

$$\min_a \sum_{i=1}^{q} a_i^2\left(1 - \frac{\omega_m^2}{\omega_i^2}\right)^2 \quad \text{with } \frac{\|\mathbf{\Pi}_m\mathscr{T}\mathbf{a} - t\bar{r}\,\boldsymbol{\sigma}_m\|}{\|t\bar{r}\,\boldsymbol{\sigma}_m\|} \leqslant \varepsilon_m. \tag{29}$$

This kind of optimization is much more difficult to solve than a single function minimization. All standard methods are described in reference [11]: the Lagrange multiplier approach, the gradient projection and reduced gradient methods, as well as the feasible direction method. These techniques with n parameters are quite cumbersome. However, particularities of the location problem allows one to simplify it and to develop an efficient solution method.

It must be underlined that this new expression of the location problem involves only the stress eigenvectors and can be adapted to a classical displacement finite element model.

4.3. PARTICULARITIES OF THE CONSTRAINED LOCATION PROBLEM

Gafka and Zimmerman [13] have shown that the constrained error location problem (29) has some interesting properties:

- The cost function is convex.
- The experimental field is close to the analytical eigenmode because only the matched modes are used in the location process.
- The solution is reached on the boundary of the inequality constraint [11]. Hence, the inequality constraint can be replaced by an equality constraint.

This last assumption can easily be demonstrated. The constraint is either active or inactive. Consider these two cases.

Case 1: *The constraint is inactive*

$$\frac{\|\mathbf{\Pi}_m\mathscr{T}\mathbf{a} - t\bar{r}\,\boldsymbol{\sigma}_m\|}{\|t\bar{r}\,\boldsymbol{\sigma}_m\|} < \varepsilon_m.$$

The solution is in the admissible domain. The constraint has no influence on the solution computation and can be disregarded. The solution of the problem is then the analytical mode. This solution is only acceptable if the estimated error ε_m is greater than the distance ε_0 between the analytical and experimental data. In this case the updating process is not helpful.

Case 2: *The constraint is active*

$$\frac{\|\mathbf{\Pi}_m\mathscr{T}\mathbf{a} - t\bar{r}\,\boldsymbol{\sigma}_m\|}{\|t\bar{r}\,\boldsymbol{\sigma}_m\|} = \varepsilon_m.$$

The solution is on the boundary of the admissible domain. This is the only possibility when the first one is ruled out. The constraint compels the solution to tend towards experimental values.

Using previous particularities, the error location problem can be written:

$$\min_{a} \mathscr{F}(\mathbf{a}) \quad \text{with } \mathscr{G}(\mathbf{a}, \varepsilon_m) = 0, \tag{30}$$

$$\mathscr{F}(\mathbf{a}) = \mathbf{a}^{\mathrm{t}}\mathbf{Q}\mathbf{a} = \sum_{i=1}^{q} a_i^2 \left(1 - \frac{\omega_m^2}{\omega_i^2}\right)^2,$$

$$\mathscr{G}(\mathbf{a}, \varepsilon) = \|\mathbf{\Pi}_m \mathscr{T}\mathbf{a} - t\bar{r}\,\boldsymbol{\sigma}_m\|^2 - \varepsilon^2 \|t\bar{r}\,\boldsymbol{\sigma}_m\|^2.$$

4.3. A NEW SOLUTION PROCESS

The distance between analytical and experimental data ε is now considered as a parameter of the optimization process. To each particular value ε_m of ε, only one solution $\mathbf{a}$ corresponds. So instead of solving problem (30), the distance ε is forced to tend towards ε_m. The constrained minimization (30) can be transformed into a single minimization by introducing a Lagrange's multiplier λ:

$$\min_{a,\lambda} \mathscr{F}(\mathbf{a}) + \lambda \mathscr{G}(\mathbf{a}, \varepsilon). \tag{31}$$

The steady state condition towards λ sets the constraint on the measured data:

$$\frac{\partial}{\partial \lambda}(F + \lambda \mathscr{G}) = 0 \Rightarrow \mathscr{G}(\mathbf{a}, \varepsilon) = 0. \tag{32}$$

The steady state condition towards modal coefficients $\mathbf{a}$ provides the relationship

$$\frac{\partial}{\partial a}(F + \lambda \mathscr{G}) = 0 \Rightarrow \mathbf{grad}\,\mathscr{F}(a) = -\lambda \underset{\varepsilon = cst}{\mathbf{grad}}\, \mathscr{G}(\mathbf{a}, \varepsilon). \tag{33}$$

From this relationship, one can deduce that λ has to be positive; otherwise the constraint will not be active. Furthermore, this relationship allows one to express the parameters $\mathbf{a}$ in terms of λ:

$$\mathbf{a}(\lambda) = \lambda(\mathbf{Q} + \lambda(\mathbf{\Pi}_m \mathscr{T})^{\mathrm{t}}(\mathbf{\Pi}_m \mathscr{T}))^{-1}(\mathbf{\Pi}_m \mathscr{T})^{\mathrm{t}}\, t\bar{r}\,\boldsymbol{\sigma}_m. \tag{34}$$

By substituting this relation into equation (32), the minimization problem (31) can be transformed into solving equation (35) versus λ:

$$\mathscr{G}(\mathbf{a}(\lambda), \varepsilon_m) = 0. \tag{35}$$

This equation can also be written as

$$\varepsilon(\lambda) = \frac{\|\mathbf{\Pi}_m \mathscr{T}\mathbf{a}(\lambda) - t\bar{r}\,\boldsymbol{\sigma}_m\|}{\|t\bar{r}\,\boldsymbol{\sigma}_m\|} = \varepsilon_m. \tag{36}$$

This equation will finally be solved in terms of an iterative linearization of the distance ε versus Lagrange's multiplier. To improve the regularity of $\varepsilon(\lambda)$ and using the fact that λ was to be positive, the multiplier λ is replaced by 10^{μ}, with μ in $]-\infty, +\infty[$. The expression of the modal coefficients becomes

$$\mathbf{a}(\mu) = 10^{\mu}(\mathbf{Q} + 10^{\mu}(\mathbf{\Pi}_m\mathscr{T})^{\mathrm{t}}(\mathbf{\Pi}_m\mathscr{T}))^{-1}(\mathbf{\Pi}_m\mathscr{T})^{\mathrm{t}}\, t\bar{r}\,\boldsymbol{\sigma}_m. \tag{37}$$

For each experimental mode k, one has to solve the iterative problem defined by

$$\varepsilon(\mu_{i-1}) + (\mu_i - \mu_{i-1})\left(\frac{\partial\varepsilon}{\partial\mu}\right)_{\mu_i - 1} = \varepsilon_m. \tag{38}$$

The initial point μ_0 is computed with the analytical mode, normalized towards the experimental data:

$$\mu_0 = \log\left(\frac{\|\mathbf{Q}\mathbf{a}_0\|}{\|(\mathbf{\Pi}_m\mathscr{T})^{\mathrm{t}}(\mathbf{\Pi}_m\mathscr{T}\,\mathbf{a}_0 - tr\,\boldsymbol{\sigma}_m)\|}\right) \quad \text{with } a_0^{(j)} = \frac{(\mathbf{\Pi}_m\mathscr{T}_k)^{\mathrm{t}}\, t\bar{r}\,\boldsymbol{\sigma}_m}{(\mathbf{\Pi}_m\mathscr{T}_k)^{\mathrm{t}}(\mathbf{\Pi}_m\mathscr{T}_k)}\,\delta_{jk}.$$

The solution of equation (38) requires the sensitivity computation of ε versus μ. Define

$$\mathbf{A}(\mu) = (\mathbf{Q} + 10^{\mu}(\mathbf{\Pi}_m\mathscr{T})^{\mathrm{t}}(\mathbf{\Pi}_m\mathscr{T})), \tag{39}$$

$$\frac{\partial\mathbf{A}^{-1}}{\partial\mu} = -\,\mathbf{A}^{-1}\frac{\partial\mathbf{A}}{\partial\mu}\mathbf{A}^{-1} \Rightarrow \frac{\partial\mathbf{A}^{-1}}{\partial\mu} = -\ln(10)10^{\mu}\mathbf{A}^{-1}(\mathbf{\Pi}_m\mathscr{T})^{\mathrm{t}}(\mathbf{\Pi}_m\mathscr{T})\mathbf{A}^{-1}. \tag{40}$$

The sensitivity expression is then

$$\frac{\partial\varepsilon}{\partial\mu} = \frac{1}{2\varepsilon}\frac{\partial\varepsilon^2}{\partial\mu}, \tag{41}$$

$$\frac{\partial\varepsilon^2}{\partial\mu} = 2\,\frac{(\mathbf{\Pi}_m\mathscr{T}\,\mathbf{a} - t\bar{r}\,\boldsymbol{\sigma}_m)^{\mathrm{t}}\mathbf{\Pi}_m\mathscr{T}}{t\bar{r}\,\boldsymbol{\sigma}_m^{\mathrm{t}}\, t\bar{r}\,\boldsymbol{\sigma}_m}\,\frac{\partial\mathbf{a}}{\partial\mu}, \tag{42}$$

$$\frac{\partial\mathbf{a}}{\partial\mu} = \ln(10)10^{\mu}\mathbf{A}^{-1}(I - 10^{\mu}(\mathbf{\Pi}_m\mathscr{T})^{\mathrm{t}}(\mathbf{\Pi}_m\mathscr{T})\mathbf{A}^{-1})(\mathbf{\Pi}_m\mathscr{T})^{\mathrm{t}}\, t\bar{r}\,\boldsymbol{\sigma}_m. \tag{43}$$

Even if the previous expression seems to be complex, it involves only small matrices of order n (length of the modal basis). The solution of this new location problem is very fast and the convergence is achieved in a few steps (see Figure 2). Error indicators are then computed using expressions (16) or (23). The key point of this method is the choice of the measurement error ε_m, according to the projection error ε_p and the initial distance between analytical and experimental data ε_0. The influence of this choice on the error location will be investigated later.

5. OPTIMIZATION PROCESS

The ability to understand all possible error causes requires experience in updating problems, as well as good knowledge of the modelling hypothesis and

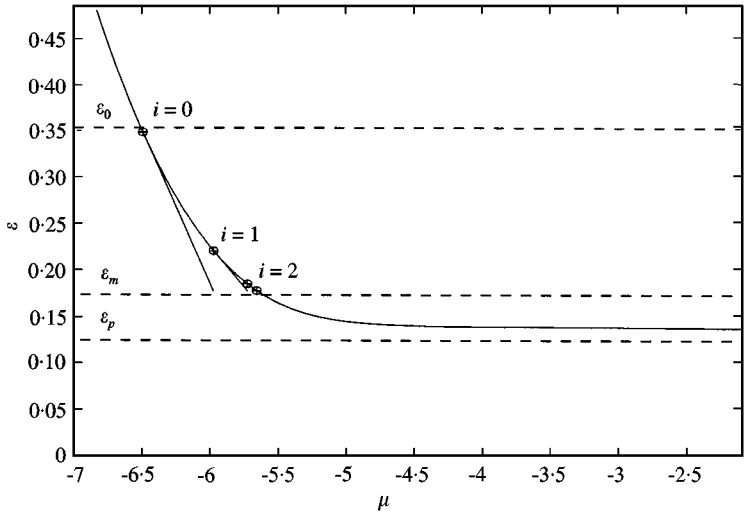

Figure 2. Solution for the first mode.

the mechanical behaviour of the experimental structure. Error indicators do not give any information about the kind of modelling error. However, depending on the structure area highlighted by error indicators, it is often possible to guess parameters that affect the modelling most.

The mass and stiffness of the finite element or group of elements, as well as boundary stiffnesses have been taken as optimization parameters. All geometrical parameters can be managed in this way:

$$\mathbb{M} = \mathbb{M}_0 + \sum_{i=1}^{\cdots} p_i^{\mathbb{M}} \mathbb{M}^{(i)}, \qquad \mathbb{K} = \mathbb{K}_0 + \sum_{i=1}^{\cdots} p_i^{\mathbb{K}} \mathbb{K}^{(i)}. \tag{44}$$

The choice of the cost function has been widely discussed in the literature [5, 11, 14]. This function can involve the error between analytical and experimental eigenfrequencies or mode shapes, modal analysis criterion coefficients, residual forces, constitutive law error or a linear combination of this data. Thermoelastic mode shapes and eigenfrequencies have been introduced by means of the distance between analytical and experimental data. The advantage of this choice is to improve the model using untreated data, but supplying a highly non-linear cost function.

$$\mathscr{F}(p_i^M, p_i^K) = \sum_{k=1}^{m} \frac{\|\mathbf{\Pi}_m T_r \mathbf{\Sigma}_k - t\bar{r}\,\boldsymbol{\sigma}_{km}\|}{\|t\bar{r}\,\boldsymbol{\sigma}_{km}\|} + \frac{\|\omega_k^2 - \omega_{km}^2\|}{\omega_{km}^2}. \tag{45}$$

The minimization of this cost function is achieved by means of a metric variable quasi-Newton process [11] with a polynomial line search. The gradient is computed using a modal parameter sensitivity method. As the function is non-linear and the parameters may have different rank orders, the gradient is corrected through iterative estimation of the Hessian with the Davidon Fletcher Powell

method. Then the minima in this direction are searched through polynomial approximation of the correction step length. When the minima are reached, another search direction is computed. If there are no local minima the algorithm must converge [15]. To avoid convergence problems due to local minima some regularization methods have been developed [14]. In the present case, it is assumed that the amount of experimental thermoelastic data and the summation on many modes provides a regular enough function. However, to avoid a divergence of the finite element solution, the parameter changes have been limited to *a priori* estimated range. This optimization method, based on an iterative linearization of the cost function, calls for modal parameter derivatives versus structural parameters:

$$\frac{\partial \mathscr{F}}{\partial p} = \frac{\partial \mathscr{F}}{\partial \Sigma_k}\frac{\partial \Sigma_k}{\partial p} + \frac{\partial \mathscr{F}}{\partial \omega_k^2}\frac{\partial \omega_k^2}{\partial p}. \tag{46}$$

For a standard model, the derivatives of the modal stresses can be computed only by finite difference methods, which require a lot of model evaluations. The use of a mixed model allows quick computation of these derivatives. The modal parameter sensitivities versus structural parameters are obtained by differentiating the governing mixed equations (47) and (48) versus these parameters:

$$\begin{pmatrix} -\omega_k^2 \mathbb{M} & \mathbb{K}_1 \\ \mathbb{K}_1^{\mathrm{t}} & \mathbb{K}_2 \end{pmatrix} \begin{pmatrix} \boldsymbol{\phi}_k \\ \boldsymbol{\Sigma}_k \end{pmatrix} = \begin{pmatrix} \mathbf{0} \\ \mathbf{0} \end{pmatrix}. \tag{47}$$

$$\text{with } \boldsymbol{\phi}_k^{\mathrm{t}} \mathbb{M} \boldsymbol{\phi}_h = \delta_{kh} \tag{48}$$

$$\Rightarrow -\omega_k^2 \mathbb{M}\frac{\partial \boldsymbol{\phi}_k}{\partial \mathbf{p}} + \mathbb{K}_1 \frac{\partial \boldsymbol{\Sigma}_k}{\partial \mathbf{p}} - \frac{\partial \omega_k^2}{\partial \mathbf{p}} \mathbb{M}\boldsymbol{\phi}_k = \omega_k^2 \frac{\partial \mathbb{M}}{\partial \mathbf{p}} \boldsymbol{\phi}_k - \frac{\partial \mathbb{K}_1}{\partial \mathbf{p}} \boldsymbol{\Sigma}_k, \tag{49}$$

$$\mathbb{K}_1^{\mathrm{t}} \frac{\partial \boldsymbol{\phi}_k}{\partial \mathbf{p}} + \mathbb{K}_2 \frac{\partial \boldsymbol{\Sigma}_i}{\partial \mathbf{p}} = -\frac{\partial \mathbb{K}_1}{\partial \mathbf{p}} \boldsymbol{\phi}_k - \frac{\partial \mathbb{K}_2}{\partial \mathbf{p}} \boldsymbol{\Sigma}_k, \tag{50}$$

$$\boldsymbol{\phi}_k^{\mathrm{t}} \frac{\partial \mathbb{M}}{\partial \mathbf{p}} \boldsymbol{\phi}_k + 2\boldsymbol{\phi}_k^{\mathrm{t}} \mathbb{M} \frac{\partial \boldsymbol{\phi}_k}{\partial \mathbf{p}} = \mathbf{0}. \tag{51}$$

For single eigenvalues, previous relationships are sufficient to determine modal sensitivities. The exact solution by means of Nelson's method has a too high computational cost to be applied. So the Fox's modal superposition method [12], which consists of representing the displacement and stress sensitivities by contributions of the q first eigenvectors has been adapted:

$$\frac{\partial \boldsymbol{\phi}_k}{\partial \mathbf{p}} = \boldsymbol{\Phi}\mathbf{a}, \qquad \frac{\partial \boldsymbol{\Sigma}_k}{\partial \mathbf{p}} = \boldsymbol{\Sigma}\mathbf{b}. \tag{52}$$

The coefficients a_i and b_i (i in $[1, n]$) are determined by premultiplying equations (49)–(51) with $\boldsymbol{\phi}_i$ and $\boldsymbol{\Sigma}_i$, and using the orthogonality properties. The final outcome

is that

$$\frac{\partial \omega_k^2}{\partial \mathbf{p}} = -\,\boldsymbol{\phi}_k^{\mathrm{t}}\,\mathbf{f}_1 - \boldsymbol{\Sigma}_k^{\mathrm{t}}\,\mathbf{f}_2, \tag{53}$$

$$a_i = \begin{cases} \dfrac{\boldsymbol{\phi}_k^{\mathrm{t}}\,\mathbf{f}_1 + \boldsymbol{\Sigma}_k^{\mathrm{t}}\,\mathbf{f}_2}{\omega_i^2 - \omega_k^2}, & i \neq k, \\ -\,1/2\boldsymbol{\phi}_k^{\mathrm{t}}\dfrac{\partial \mathbf{M}}{\partial \mathbf{p}}\,\boldsymbol{\phi}_k, & i = k, \end{cases} \tag{54}$$

$$b_i = a_i - \frac{\boldsymbol{\phi}_i^{\mathrm{t}}\,\mathbf{f}_2}{\omega_i^2}. \tag{55}$$

with

$$\mathbf{f}_1 = \omega_k^2\,\frac{\partial \mathbb{M}}{\partial \mathbf{p}}\,\boldsymbol{\phi}_k - \frac{\partial \mathbb{K}_1}{\partial \mathbf{p}}\,\boldsymbol{\Sigma}_k \quad \text{and} \quad \mathbf{f}_2 = -\,\frac{\partial \mathbb{K}_1^{\mathrm{t}}}{\partial \mathbf{p}}\,\boldsymbol{\phi}_k - \frac{\partial \mathbb{K}_2}{\partial \mathbf{p}}\,\boldsymbol{\Sigma}_k.$$

This method requires very little computation, but has frequently been shown to be inaccurate due to the use of an incomplete set of eigenvectors in the expansion [12]. Other techniques, such as the Zhang and Zerva iterative method or preconditioned conjugate projected gradient iterative technique [12], allow one to improve derivative calculation but introduce high computation. Nevertheless, the accuracy of Fox's method can be improved by increasing the number of eigenvectors. Moreover, as the correction is done by using an iterative method, one assumes that high accuracy is not necessary.

6. EXPERIMENTAL RESULTS

6.1. THERMOELASTIC MEASUREMENT OF THIN PLATE BENDING

The measurement of the dilatation temperature change is made without contact, at room temperature, by means of a thermographic camera (SPATE 4000 Ometron) fitted with a mirror scanning system. It allows one to obtain a wide experimental field on the tested structure area at fixed frequencies (here the eigenmode thermoelastic fields). The thermoelastic information, which is about 0·01–0·5 K, is extracted from the other room temperature changes through a frequential analytical filtering. The measurement is fully controlled by a computer (see Figure 3).

All physical phenomena involved in this measurement technique, such as the infrared emissivity, the gaseous media absorption, the radiation detection, as well as the thermoelastic signal calibration, were investigated in detail in reference [2]. The accuracy of temperature measurement reaches almost 0·001 K, which corresponds to a stress level of about 1·0 MPa for steel and 0·4 MPa for aluminium. The main limitation of this technique is the stress level one is able to generate, especially for high frequencies.

Thermoelastic modal measurements were carried out on a thin aluminium plate, with free-clamped boundary conditions (Figure 4). Different kinds of defects were

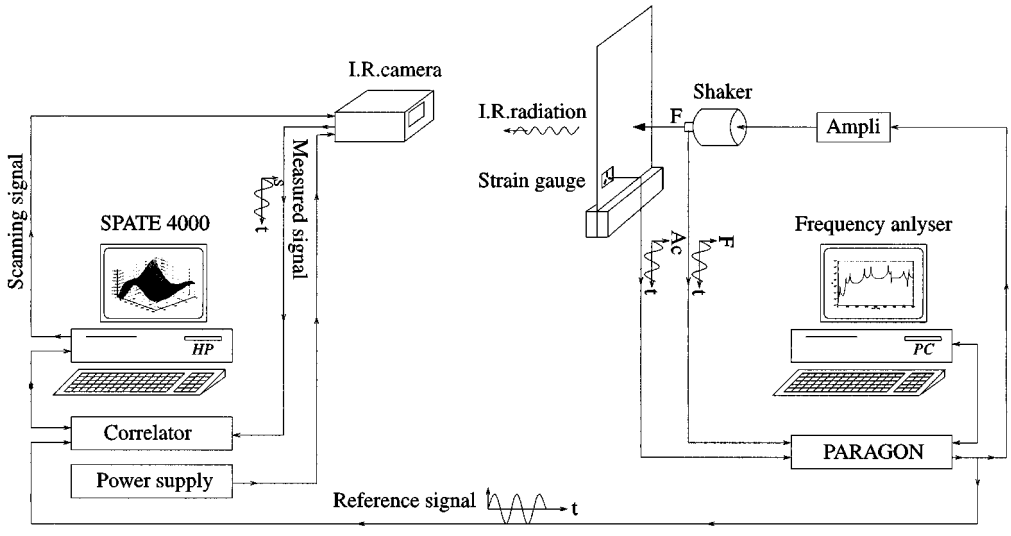

Figure 3. Experimental set-up.

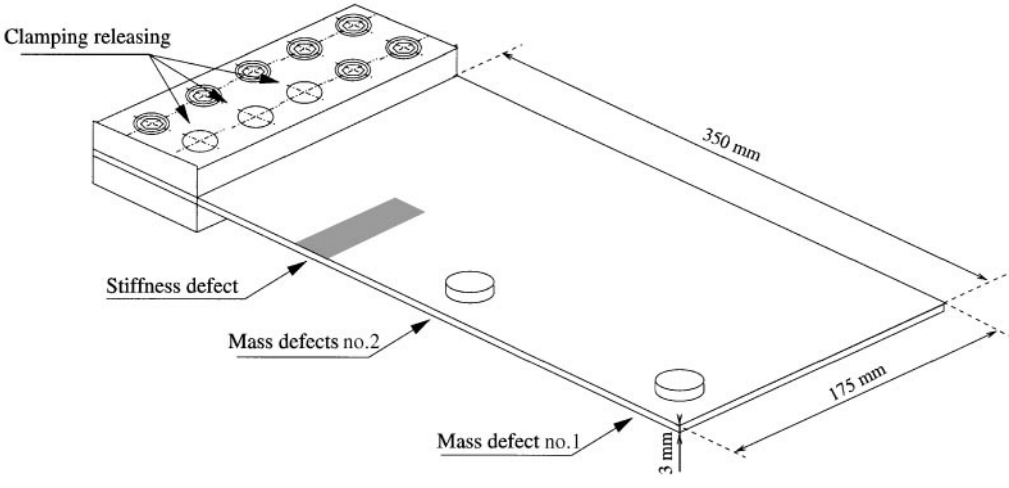

Figure 4. Experimental structure.

tested, successively: a 38 g mass located at different positions, a material damage (a set of little borings) reducing the stiffness by about 30%, and releasing of clamped boundary conditions. For the latter defect some screws were removed. The excitation was realized with a shaker controlled by a frequency analyzer. A modal analysis was carried out in order to detect the first modes of the plate with a high accuracy. The thermoelastic measurement does not allow modal extraction. However, as the modes are well separated and the damping is small, one can consider that the measured shape can be compared with its mode shape.

Figure 1 shows the thermoelastic modal measurements for the first four modes. The experimental fields have been obtained on a mesh involving $36 * 74$ points and

are quite smooth. The thermoelastic field was calibrated by a strain gauge stuck on the rear side of the plate.

6.2. KIRCHOFF'S THIN PLATE MODELLING

The plate can be modelled with a different kind of approach [3, 4]. A choice was made to model it with a two-field Hellinger–Reissner formulation and Kirchoff's thin plate hypothesis. Major assumptions of this theory are that: plane sections remain plane during deformation, the bending and membrane behaviours can be dealt separately, the direct stress in the normal direction σ_z is small enough to be neglected, together with the shear deformation. The behaviour of the plate can then be described by the normal displacement u of the middle plane and the bending moments $(\tilde{\sigma}_x, \tilde{\sigma}_y, \tilde{\sigma}_{xy})$:

$$\bar{\sigma} = \int_{-e/2}^{e/2} z\sigma \, \mathrm{d}z = \begin{pmatrix} \bar{\sigma}_x \\ \bar{\sigma}_y \\ \bar{\sigma}_{xy} \end{pmatrix}. \tag{56}$$

The finite element mesh (Figure 5) is composed of 231 rectangular elements with four nodes per element. Convergence problems of mixed formulations are discussed in reference [3]. They lead to some requirements linking the respective number of displacement and stress degrees of freedom. To avoid this difficulty the same order approximation that requires four degrees of freedom per element was taken for all displacements and stress components. So, four degrees of freedom are defined for each node: one displacement $\bar{u}$ and three bending moments $\bar{\sigma}_x$ $\bar{\sigma}_y$ $\bar{\sigma}_{xy}$. This modelling leads to a set of equations which have the same expression as (2).

The clamped edge is generally obtained by setting corresponding generalized degrees of freedom to zero. Nevertheless, a real clamping never has infinite rigidity.

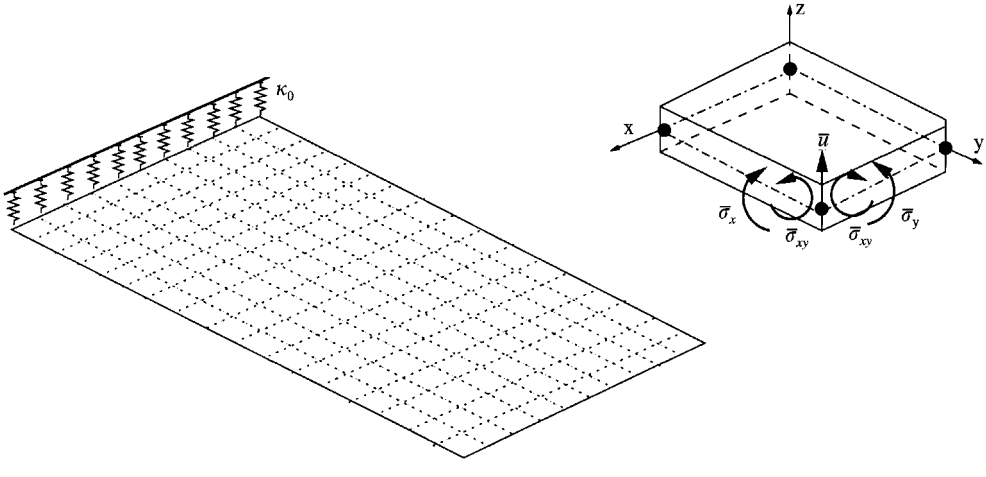

Figure 5. Finite element model.

So it was modelled by a set of linear springs k_0, that will be updated in the correction step. These springs are introduced in the mixed formulation by means of their potential energy $k_0 u^2$ and will finally appear as k_0 diagonal terms associated with the corresponding displacement degrees of freedom.

For bending deformation the stress distribution is linear; so bending moments can be directly related to the top area stresses by

$$\sigma_{(z=e/2)} = \pm\, e/2\tilde{\sigma} \tag{57}$$

$$\Rightarrow tr\,\tilde{\sigma}_m = \pm\, 2/e\, tr\,\sigma_m. \tag{58}$$

The thermoelastic values were then projected on to the mesh using the finite element shape functions (10), to obtain corresponding degrees of freedom $tr\,\bar{\varepsilon}_m$.

6.3. ERROR LOCATION

The previous model has been used to compute 30 displacement and stress sum mode shapes $(\omega_i, \boldsymbol{\phi}_i, \mathscr{T}_i)$, useful for the location process. Before beginning the updating, the distance between experimental and analytical values as well as the error introduced by the modal subspace (28) were estimated. Table 1 shows these data for the first mass defect.

The expansion error is about 10% and is thus significant, in comparison with the modelling error. The convergence rate of the modal projection is very low and a basis of 50 modes only reduces this error by 1 or 2%. The measurement error is estimated *a priori* to be around 5%, to which is added the expansion error ε_p to obtain the constraint ε_m. The convergence of the constrained location method is very fast and is reached in a few steps, as shown in Figure 2. On this curve, the distance ε in terms of μ and successive iterations of the resolution were plotted. When μ increases, it enforces the experimental term of equation (31) and ε tends toward ε_p.

Figure 6 shows modal error location for the first mass defect. The location is not very good. Not only has the mass been located, but also other parts of the structure.

Due to expansion or measurement errors the ill-modelled area is never located by a single peak. The modelling error may not affect all modes or can be hidden by measurement errors or be filtered by the modal basis. Furthermore, the effect of an erroneous parameter on the dynamic response varies with the frequency domain and the parameter type.

The ill-modelled parameter detection consists in finding areas appearing on many indicators. This is quite easy in the case of a numerical simulation especially when the modelling error is known, but proves much more difficult in a real case. Usually, the normalized indicators are simply added (59) and provide a global indicator for all the modes:

$$\chi_1^{(e)} = \sum_{k=1}^{m} \frac{\eta_k^{(e)}}{\|\eta_k\|}. \tag{59}$$

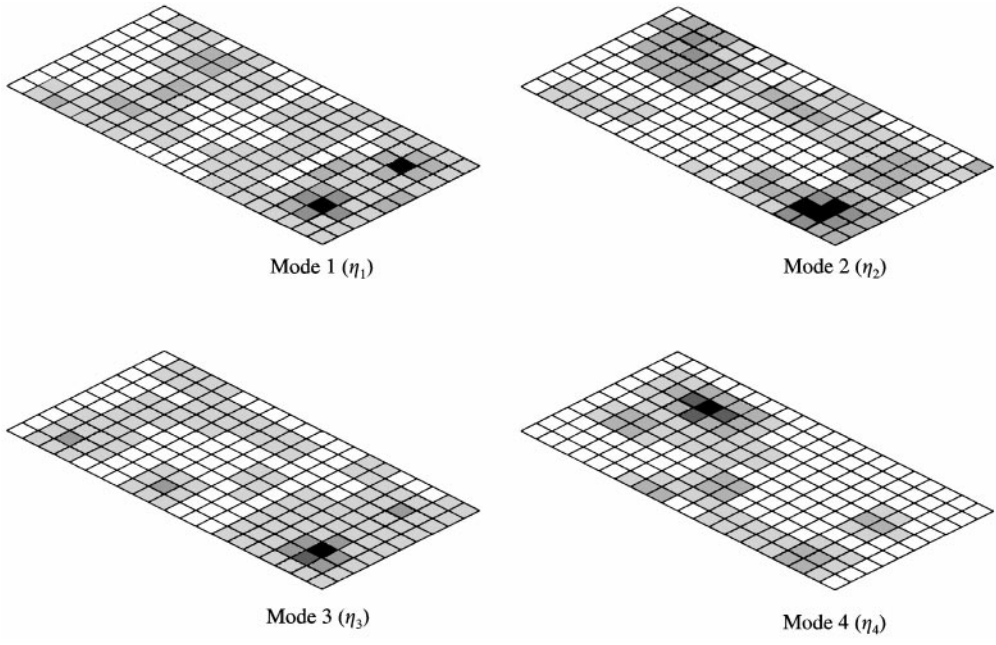

Figure 6. Error location for the mass defect.

In reference [16], the author suggests weighting the frequency location indicators by the dissipated energy. Another approach has been chosen which uses a correlation between all modal indicators (60), which highlights errors occurring on many indicators:

$$\chi_2^{(e)} = \sum_{k,h=1\ k\neq h}^{m} \frac{\eta_k^{(e)}\eta_h^{(e)}}{\|\eta_k\|\,\|\eta_h\|}. \tag{60}$$

Figure 7 shows the indicator χ_2 carried out for all considered defects, with the first four thermoelastic measurements. All kinds of defects are located with good accuracy. However, it is noteworthy that the excitation area is detected too. This technique is very interesting when experimental information is available for a lot of frequency points and when the measurement error is significant. The discrimination capacity of these correlated indicators is greater than the standard ones.

The solution of the location process is directly determined by the enforced error ε_m. This parameter seems to be very important, but it cannot be estimated with high accuracy. It is usually given *a priori*, according to the measurement quality. Hence, the sensitivity of the location versus this parameter has been investigated. In Figure 8, is plotted the constitutive law error versus the multiplier μ and versus ε_m, and the location of its approximate domain is achieved.

The location is achieved for a quite large domain of μ and ε_m. However, these domains are not the same for each mode. When μ becomes too great, the energy $E^2(\bar{\mathbf{u}}, \bar{\mathbf{v}})$ increases quickly and the location fails. This corresponds to a decrease in the distance between experimental and analytical data, ε, which tends towards ε_p.

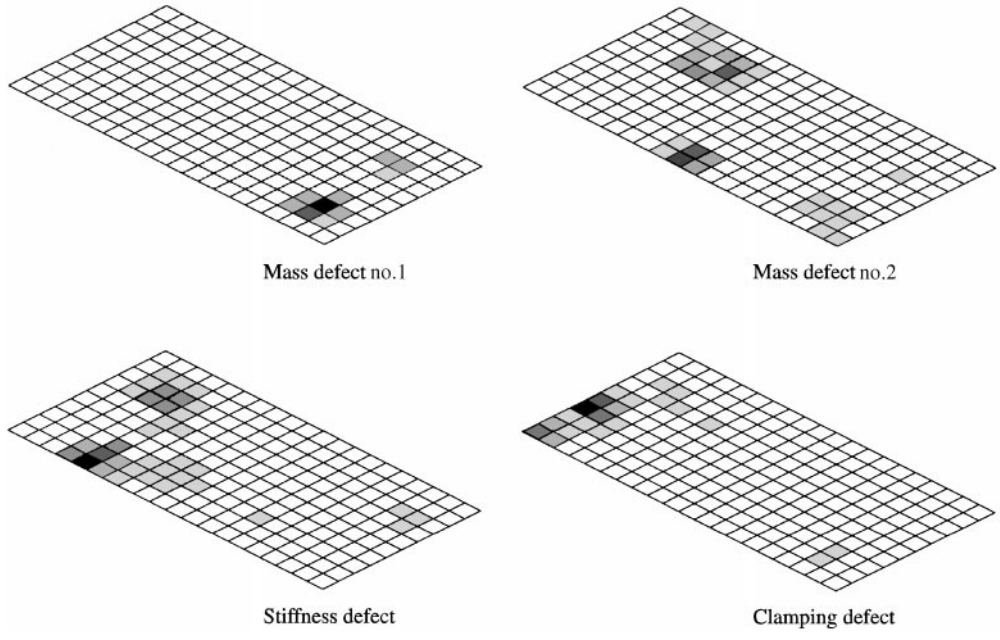

Figure 7. Error location using χ_2.

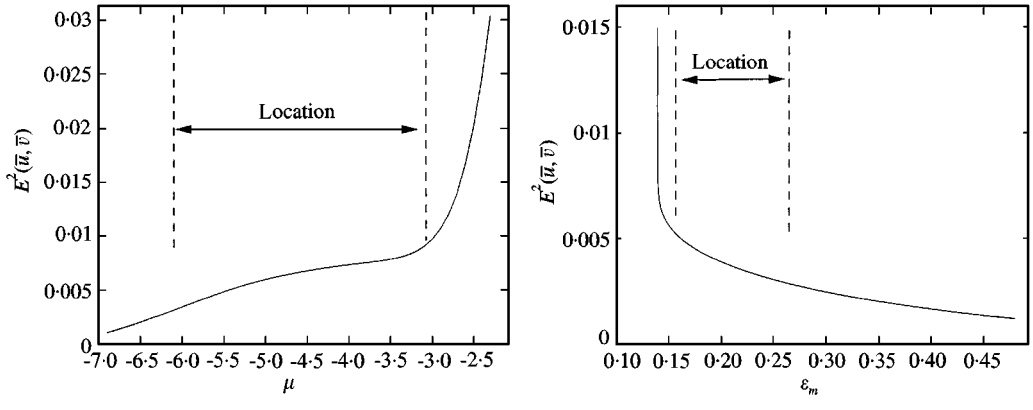

Figure 8. Constitutive law error (first mode).

The parameter μ enforces the measurement inaccuracies too. Since measurement errors have a greater deformation energy than modelling errors, the constitutive law error increases faster. Thus, the optimal measurement expansion is obtained for the upper bound of μ's location domain.

6.4. MODEL OPTIMIZATION

Now consider the results of the model correction for the first mass defect. This defect is represented by mass m at the position located by indicator χ_2 (Figure 7). The clamped edge is split into three parts with a stiffness parameter α_i for each one.

Boundary stiffnesses were introduced using power parameters to improve their linearity,

$$k'_{0i} = 10^{\alpha_i} k_{0i}. \tag{61}$$

The optimization requires 12 sensitivity computations and about 40 evaluations of the finite element model. It leads to a cost function monotonic decrease of 56%. But as shown in Figures 9(b) and 9(c), different terms of the cost function (45) have

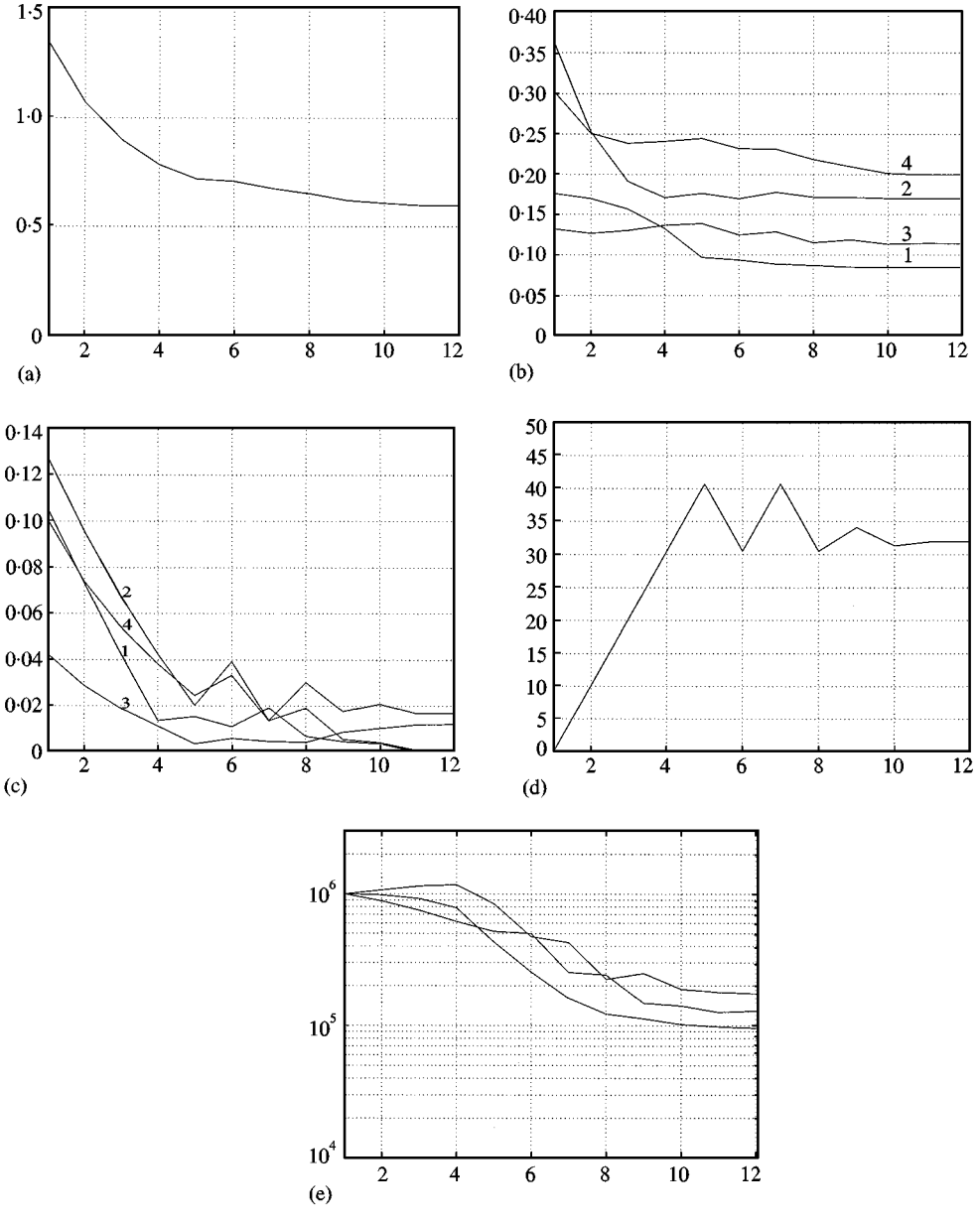

Figure 9. Correction of the mass defect: (a) cost function; (b) error on thermoelastic fields; (c) error on eigenfrequencies; (d) mass parameter m (10^{-3} kg); (e) boundary stiffnesses k_{0i} (N/m).

TABLE 2

Correction of modal parameters

Mode		1	2	3	4
Eigenfrequency	(%)	98	87	71	98
Thermoelastic data	(%)	52	53	14	34

a less regular trend. The observable chaotic and irregular behaviours are due to the strong cost function non-linearities. The correction ratio of modal eigenfrequencies and thermoelastic data are given in Table 2.

The mass defect is updated by about 85% and the boundary stiffnesses are reduced from the $10^6\ \mathrm{N\,m^{-1}}$ initial value to about $10^5\ \mathrm{N\,m^{-1}}$. The residual error on thermoelastic modal fields is due to either thermoelastic measurement inaccuracies or physical phenomena which have not been modelled. Nevertheless, the model improvement is quite significant and shows the usefulness of thermoelastic data in the correction step.

7. CONCLUSION

The aim of this paper was not to promote thermoelasticity as the best experimental information for finite element updating, but to show that it can be successfully used to achieve this goal. Measurements are usually the last stage of the design process and are rarely planned for updating purposes. So the user cannot choose the experimental data, which could be displacement as well as stress values. Moreover, finite element models are usually used to predict the stress level; it can also be interesting to update them with respect to this kind of data.

So far the lack of experimental data has put a curb on updating methods, but modern experimental techniques enable now a wide and accurate measure of the real behaviour of mechanical structures. The new approach of the modelling error location has a better accuracy and robustness to measurement errors than the standard one. The single parameter of the location problem is now the *a priori* measurement error which is easier to estimate than the former weighting factor and has a physical meaning. Moreover, the introduction of a correlation between modal error indicators already improves the detection of ill-modelled parameters. This should be stressed.

The use of non-standard mixed models could be a drawback because this kind of modelling is not available in industrial finite element softwares. However, the solution by means of a modal superposition technique involves only stress eigenvectors (see equation (29)) which can be estimated with most of the classical softwares. Nevertheless, the so obtained stress vectors are generally less accurate than those computed using a mixed model and do not necessarily satisfy static

boundary conditions. Finally, it must be underlined that the present developments are not limited to the use of thermoelastic data. The new solution technique proposed can be applied to any standard expansion and location methods based on the constitutive law error or the residual forces.

REFERENCES

1. A. S. Kobayashi 1998 *Handbook on Experimental Mechanics*, 581–597. SEM.
2. N. Harwood and W. M. Cummings 1986 *NEL Report No.* 705. Calibration and Qualitative Assesment of the SPATE stress measurement system.
3. O. C. Zienkiewicz and R. L. Taylor 1994 *The Finite Element Method*. New York: McGraw-Hill.
4. F. Brezzi and M. Fortin 1991 *Mixed and Hybrid Finite Element Methods*. Berlin: Springer-Verlag.
5. M. I. Friswell and J. E. Mottershead 1995 *Finite Model Updating in Structural Dynamics*. Dordrecht: Kluwer Academic Publishers.
6. M. Baruch 1978 *AIAA Journal* **16**. Optimisation procedure to correct stiffness and flexibility matrices using vibration data.
7. A. M. Kabe 1985 *AIAA Journal* 23. Stiffness matrix adjustment using modal data.
8. F. M. Hemez and C. Farhat 1995 *Journal of Modal Analysis* 10, 152–166. Structural damage detection via finite element model updating methodology.
9. P. Ladeveze and M. Reynier 1989 *12th ASME Mech. Vibration and Noise Conference, Montreal*. A localization method of stiffness errors for adjustment of finite element models.
10. P. Collignon and J. C. Golinval 1995 *Proceedings of Congres MV2*. Comparison of experimental eigenvector expansion methods for failure detection.
11. R. T. Haftka, Z. Gurdal and M. P. Kamat 1990 *Element of Structural Optimisation*. Dordrecht: Kluwer Academic Publishers.
12. K. F. Alvin 1998 *Proceedings of IMAC Conferences*, 652–659. Efficient computation of eigenvector sensitivities for structural dynamics via conjugate gradients.
13. G. K. Gafka and D. C. Zimmerman 1997 *Proceedings IMAC*, 1278–1284. Model updating using constrained eigenstructure assignment.
14. A. Tarantola 1987 *Inverse Problem Theory, Methods for Data Fitting and Model Parameter Estimation*. Amsterdam: Elsevier.
15. G. H. T. Ng and J. E. Mottershead 1995 *Proceedings of IMAC Conferences*, 1282–1288. Model updating by a two level Gauss–Newton approach with line searching.
16. A. Chouaki 1997 *Ph.D. Thesis, LMT ENS Cachan, France*. Une méthode de recalage des modèles dynamiques des structures avec amortissement.

APPENDIX A: HELLINGER–REISSNER MIXED MODEL

The approximated mechanical fields are given for each element (e) versus degrees of freedom at every node n by

$$u^{(e)}(x, y, z) = \sum_n N_{un}^{(e)}(x, y, z)\bar{u}_n^{(e)} = \mathbf{N}_u^{(e)}\bar{\mathbf{u}}^{(e)},$$

$$\sigma^{(e)}(x, y, z) = \sum_n N_{\sigma n}^{(e)}(x, y, z)\bar{\sigma}_n^{(e)} = \mathbf{N}_\sigma^{(e)}\bar{\sigma}^{(e)}.$$

For a two-field ($\mathbf{u} - \boldsymbol{\sigma}$) formulation, Zienkiewicz and Taylor [3] express the general expression of elementary mass and stiffness matrices:

$$\mathbf{M}^{(e)} = \int_{\Omega_e} \rho \mathbf{N}_u^{(e)} \mathbf{N}_u^{(e)\mathrm{t}} \, \mathrm{d}x \, \mathrm{d}y,$$

$$\mathbf{K}_1^{(e)} = \int_{\Omega_e} \mathbf{N}_\sigma^{(e)} \mathbf{D} \mathbf{N}_u^{(e)\mathrm{t}} \, \mathrm{d}x \, \mathrm{d}y,$$

$$\mathbf{K}_2^{(e)} = - \int_{\Omega_e} \mathbf{N}_\sigma^{(e)} \mathbf{H}^{-1} \mathbf{N}_\sigma^{(e)\mathrm{t}} \, \mathrm{d}x \, \mathrm{d}y,$$

$$\mathbf{F}^{(e)} = \int_{\Gamma_e} t^0 \mathbf{N}_u^{(e)\mathrm{t}} \, \mathrm{d}s.$$

For the thin plate model used in the experimental part, both displacement and stress approximations are based on the same Lagrange's shape function order 1 ($N_u^{(e)} = N_\sigma^{(e)} = N$). The plate has been modelled by means of four-node rectangular elements with four-degrees-of-freedom per node: one normal displacement $\bar{u}_n$ and three bending moments $\bar{\sigma}_{xn}$, $\bar{\sigma}_{yn}$, $\bar{\sigma}_{xyn}$. The particular expression of the elementary mass and stiffness matrices are then given by

$$M_{(ij)}^{(e)} = \int_{\Omega_e} \rho e \mathbf{N}_i^{(e)} \mathbf{N}_j^{(e)} \, \mathrm{d}x \, \mathrm{d}y,$$

$$\mathbf{K}_1^{(e)} = (K_{11}^{(e)} \quad K_{12}^{(e)} \quad K_{13}^{(e)}),$$

$$\mathbf{K}_2^{(e)} = \begin{pmatrix} K_{22}^{(e)} & K_{23}^{(e)} & 0 \\ K_{23}^{(e)} & K_{33}^{(e)} & 0 \\ 0 & 0 & K_{44}^{(e)} \end{pmatrix}$$

with

$$K_{11(ij)}^{(e)} = \int_{\Omega_e} \frac{\partial N_i}{\partial x} \frac{\partial N_j}{\partial x} \, \mathrm{d}x \, \mathrm{d}y, \qquad K_{12(ij)}^{(e)} = \int_{\Omega_e} \frac{\partial N_i}{\partial y} \frac{\partial N_j}{\partial y} \, \mathrm{d}x \, \mathrm{d}y$$

$$K_{13(ij)}^{(e)} = \int_{\Omega_e} \left(\frac{\partial N_i}{\partial x} \frac{\partial N_j}{\partial y} + \frac{\partial N_i}{\partial y} \frac{\partial N_j}{\partial x} \right) \mathrm{d}x \, \mathrm{d}y$$

$$K_{22(ij)}^{(e)} = - S_{22} \int_{\Omega_e} N_i N_j \, \mathrm{d}x \, \mathrm{d}y, \qquad K_{23(ij)}^{(e)} = S_{12} \int_{\Omega_e} N_i N_j \, \mathrm{d}x \, \mathrm{d}y$$

$$K_{33(ij)}^{(e)} = - S_{11} \int_{\Omega_e} N_i N_j \, \mathrm{d}x \, \mathrm{d}y, \qquad K_{44(ij)}^{(e)} = - S_{33}^{-1} \int_{\Omega_e} N_i N_j \, \mathrm{d}x \, \mathrm{d}y$$

$$\mathbf{S} = \mathbf{H}^{-1} = \frac{12(1 - \nu^2)}{e^3 E} \begin{pmatrix} 1 & \nu & 0 \\ \nu & 1 & 0 \\ 0 & 0 & 1/2(1 - \nu) \end{pmatrix}^{-1}$$

and e the thickness of the plate.

APPENDIX B: NOMENCLATURE

c_ε, c_σ	specific heat coefficients
$\mathbf{D}$	spatial differentiation operator
E	Young's modulus
$\mathbf{H}$	Hooke's elasticity matrix
k	heat conduction
$K = \lambda + \frac{2}{3}\mu$	bulk modulus
$\mathbb{K}$, $\mathbb{M}$	stiffness and mass matrices
r	external heat supply
$tr\,\boldsymbol{\sigma}_m$	thermoelastic measurement
$tr\,\boldsymbol{\sigma}$, $tr\,\boldsymbol{\varepsilon}$	sum of the principal stresses, sum of the principal strains
T	absolute temperature
T_r	sum of the principal components
u_i, ε_{ij}, σ_{ij}	displacement, strain and stress fields
$W(\varepsilon_{ij})$	strain energy
$W_c(\sigma_{ij})$	complementary energy

Greek characters

α	dilatation coefficient
θ	temperature change
λ, μ	Lame's coefficients
ν	The Poisson ratio
$\boldsymbol{\Pi}_m$	measurement location matrix
$\boldsymbol{\Phi}$, $\boldsymbol{\Sigma}$	matrices of the q first modal deformation shapes and stress vector
ρ	mass density
$(\omega_k, \boldsymbol{\phi}_k)$	kth analytical mode
$(\omega_{km}, \mathbf{u}_{km})$	kth experimental mode